Equation of state for the low-pressure crystalline phase of SnI_4

Kazuhiro Fuchizaki*
Department of Physics, Ehime University, Matsuyama 790-8577, Japan

Nozomu Hamaya
Department of Physics, Ochanomizu University, Tokyo 112-8610, Japan

(Received 2 July 2011; published 7 October 2011)

The molecular crystal of tin tetraiodide is known to exhibit unusual features under pressure, such as solid-state amorphization. The low-pressure crystalline phase has a melting curve with a maximum at about 1.5 GPa, dividing the liquid phase into two states with different structures. However, the thermodynamic properties of this solid phase are still unknown. For proper thermodynamic measurements for the solid phase, we present here the Parsafar-Mason and Birch-Murnaghan-Anderson equations of state for the phase as a predecessor. The validity of the equations was confirmed by recent experimental observations. As far as can be seen from the equations of state, no remarkable anharmonic properties are expected, in the sense that the thermal pressure is well described by a linear function of temperature, i.e., αK_T (where α and K_T are the coefficient of thermal expansion and the isothermal bulk modulus, respectively) is virtually independent of temperature. In addition to the equations of state, we also report a unique means of holding a chemically active sample, which we established through the *in situ* x-ray diffraction measurements for SnI_4 at high pressures and temperatures.

DOI: 10.1103/PhysRevB.84.144105 PACS number(s): 64.30.−t, 64.30.Jk, 81.40.Vw, 61.05.cp

I. INTRODUCTION

The compression behavior related to pressure-induced solid state amorphization of SnI_4 has recently been reexamined by Grocholski *et al.*[1] up to about 20 GPa. They also reported the bulk modulus, K_{0T}, and its pressure derivative at ambient conditions, $K_0{}'_T$, which were obtained through fitting the compression data taken at room temperature (RT) to the Birch-Murnaghan equation of state (EOS).[2] This stimulated us to try constructing the EOS applicable at elevated temperatures from our own compression data accumulated during the period between 2001 and 2009. We also show a method of sample holding, which we established by trial and error over many years through *in situ* measurements of liquid SnI_4 under high pressure and temperature. The method is believed to be widely applicable, as it can stably hold even a chemically active liquid sample such as SnI_4.

We begin with a brief introduction of the properties of SnI_4, which shows interesting structural and electronic features under applied pressure. A first-order structural phase transition from the low-pressure crystalline phase (called CP-I hereafter) to a new crystalline phase (CP-II) takes place at 7.2 GPa and RT.[3] The transition is associated with metallization;[4] however the structure of CP-II has not been resolved yet. Applying further pressure induces molecular dissociation,[3] which causes amorphization at around 15 GPa[3,5,6] until an fcc-type crystalline structure (CP-III)[7] forms at 61 GPa. That is, solid-state amorphization occurs on compression prior to reentrant crystallization.

The structure of CP-I belongs to the space group $Pa\bar{3}$. No silent modes exist at Γ point, with half of them being Raman active[8] and the other half infrared active. Moreover, since both Sn and I are good scatterers of neutrons as well as x rays, the lattice dynamical properties were studied by neutron scattering in a relatively low-pressure region.[9] Although SnI_4 has been the subject of extensive experimental investigation, fundamental thermodynamic properties are still unknown, even for CP-I. The present authors found that the melting behavior of CP-I is far from ordinary,[10] in that Simon's equation[11] is no longer applicable; the melting curve exhibits a maximum at around 1.5 GPa in the pressure (p)–temperature (T) phase diagram.[12,13] The present report intends to compensate partially for the lack of essential thermodynamic data for CP-I.

The rest of the paper is organized as follows. The experimental procedure is described in Sec. II, in which we shall focus on our sample holding procedure. The unique material used as a cover at the top of a sample container is also highlighted. The EOS is constructed in Sec. III, and its validity is examined in Sec. IV. The final section is devoted to conclusions.

II. EXPERIMENTAL METHOD

A series of *in situ* synchrotron x-ray diffraction measurements were performed utilizing SMAP-II and MAX-80, cubic-type multi-anvil presses installed in BL14B1 at SPring-8 and in NE5C at KEK-AR, Japan, respectively. The measurements were done along pressure-temperature paths, extended up to about 4 GPa and 1000 K through the CP-I phase field to the liquid state. A total of 12 paths were selected, and the specific volume values of CP-I as determined from the diffraction data along the paths are provided for the analysis in the next section.

The energy-dispersive diffraction method was employed. The scattering angle was fixed to 4° for the measurements of CP-I, and to 8° for those of NaCl, the latter being used for pressure calibration. These angles were calibrated by using the nominal lattice constants, 12.273 Å for CP-I[14] and 6.402 Å for NaCl, at ambient conditions. A solid-state detector with pure Ge was used to detect scattered x-rays. Other details of the diffraction geometry, as well as the temperature control system, were basically the same as those described in Ref. 10. Note that such a setup was primarily intended for measurements of the liquid structure, and was not optimized

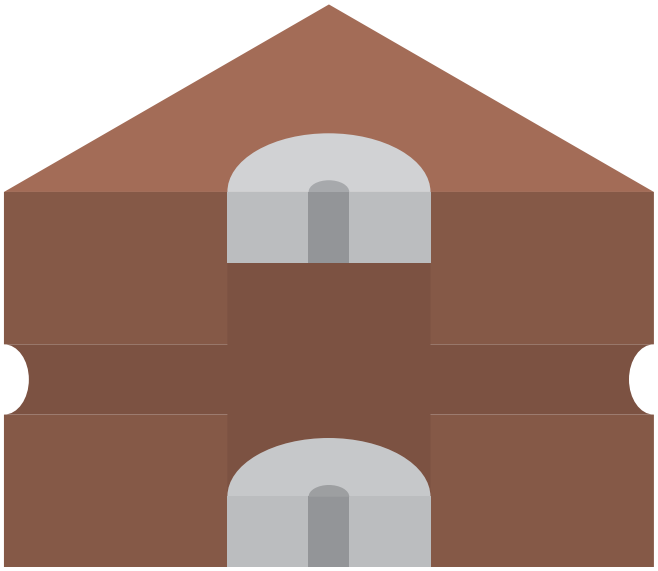

FIG. 1. (Color online) A sectional view of the cube-shaped pressure-transmitting medium. The length of an edge was 13, 9, or 7 mm, depending on the TEL of the anvils employed. The exits of a vertical hollow with a diameter of 2.5 mm were stopped by pyrophyllite plugs with a Mo electrode embedded along their central axis. The remainder of the space was filled with a graphite tube, which contained a sample container (or a pair of containers) as shown in Fig. 3 in such a way that the corundum enveloping the thermocouple just filled the horizontal hollow.

for precise determination of the lattice constant; the incident beam, passed through a horizontal slit of 200 μm width, was collimated to a width of 100 μm at the sample position. This condition ensured accuracy of the lattice constant within three digits (at best). The measurements at SPring-8 were performed using a collimator with a width of 50 μm, and the accuracy was slightly improved. See Ref. 15 for sample preparation.

Figure 1 shows a sectional view of the cube-shaped pressure-transmitting medium, made of a mixture of amorphous boron and epoxy resin in 4:1 weight ratio, used throughout the measurements. Its design was quite orthodox. The edge lengths were 13, 9, and 7 mm, depending on the truncation edge lengths (TELs) of 10, 6, and 4 mm, respectively, of the anvils employed upon compression. Pyrophyllite plugs with a Mo electrode were placed at both the top and bottom ends. The vertical hollow between the plugs contains a graphite tube (see below) covered with 0.2-mm-thick graphite disks, which acts as a heater when an electric current is turned on. A chromel-alumel or type-R thermocouple was set along the horizontal hollow.

One problem we had to cope with was the sample container, which must be transparent for x rays. It is more important, however, to choose a substance with little chemical activity with SnI_4. Before 2005, we used *h*-BN as a container. Unfortunately, however, at low scattering angles, the intense 002 reflection of *h*-BN almost overlaps with the most intense 222 reflection of CP-I (which develops into the most intense halo in the liquid state). This forced us to stop using BN, and to use diamond instead.[13] Because diamond is too hard to transmit pressure from outside, we used a sleeve so that pressure could penetrate through a hollow. However, we still had to be careful when choosing the covers. Note that a 0.2-mm-thick diamond disk was used at the bottom. Thus, the cover at the top was the only channel that could transmit pressure, and it needed to be flexible, as well as chemically inactive.

We finally arrived at pyrolytic BN (PBN), a substance that satisfies all the conditions required. Although PBN is hard at RT, it becomes flexible when the temperature exceeds about 500 K. This quite interesting feature of PBN is seen from Fig. 2, which plots $p_{\rm in}$, the internal pressure achieved in the container at various temperatures as indicated, against $p_{\rm ex}$, the external pressure applied. From the temperature dependence of the slopes, $p_{\rm in}$ is related to $p_{\rm ex}$ by the following relation:

$$p_{\rm in}({\rm GPa}) = \alpha(T) \cdot p_{\rm ex}({\rm GPa}), \tag{1a}$$

where

$$\alpha(T) \simeq \begin{cases} 2.5 \times 10^{-1} \ (T \lesssim 500 \ \ {\rm K}) \\ 1.3 \times 10^{-1} + 5.0 \times 10^{-4} T \ ({\rm K}) \ (600 \ \ {\rm K} \lesssim T \lesssim 1200 \ \ {\rm K}). \end{cases} \tag{1b}$$

At extremely high temperatures, $p_{\rm in}$ must approach $p_{\rm ex}$ from below. That is, $\alpha(T)$ in Eq. (1a) must be upper-bounded. As far as can be seen from the behavior shown by Eq. (1b), the temperatures investigated are too low for PBN to exhibit apparent deviation from linearity.

Although the problem of the sample container was resolved in this way, a new problem arose: at the temperatures of interest, the pressures inside and outside the container differed significantly. An ordinary method, in which a pressure calibrant is placed right outside (usually right below) a sample container, would no longer work, and we had to look for an alternative way to assess $p_{\rm in}$. One way in which we intended to achieve this was the configuration illustrated in Fig. 3(a). The figure depicts the graphite tube, which was meant to be placed in the vertical hollow in Fig. 1. The two identical containers, one of which contained SnI_4 while the other contained the pressure calibrant (NaCl mixed with *h*-BN), were located at the symmetrical positions about the middle intersection point with the corundum tube enveloping the thermocouple. The empty spaces within the graphite tube were filled with spacers made of *h*-BN.

We used this design from 2005 through 2008 for measuring liquids in a region near the maximum of the melting curve of CP-I. A set of anvils with a TEL of 10 mm was sufficient to access this region. In this case, a 6.4-mm-long graphite tube could accommodate two containers 1.5 mm tall. However, in order to attain a higher pressure region, anvils with a

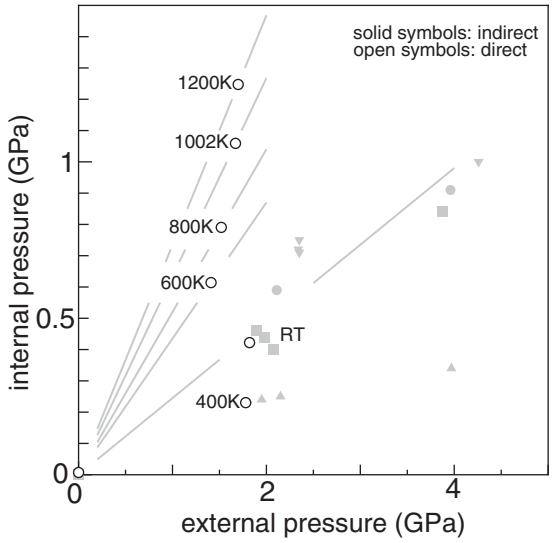

FIG. 2. Internal pressures realized within a diamond sleeve container plotted against external pressure, which is transmitted by a PBN disk placed at the top of the sleeve. The external pressure was measured by placing a pressure calibrant just below the sleeve. A blank measurement, in which the sleeve was filled with a pressure calibrant, was carried out to estimate the internal pressures marked by open circles. The solid symbols show the internal pressures determined from SnI_4 in the CP-I state using the EOS [Eq. (3)] below. The different symbols correspond to different runs. As for the scatter of the data points at RT, refer to Sec. III.

shorter TEL must be employed. This necessarily reduces the dimension of the sample assembly. For example, a typical length of a graphite tube embedded in a pressure-transmitting medium with an edge length of 9 mm is 3.6 mm, which can store only a single container at most.

To accommodate such a situation, we constructed a new assembly that contains only a single diamond sleeve as a sample container. The hollow of the sleeve was divided by a thin (0.1 or 0.2 mm thick) diamond disk into two rooms, the upper and the lower compartments being occupied by a pressure calibrant and SnI_4, respectively,[16] as shown in Fig. 3(b). Another diamond disk with a larger diameter was used at the bottom of the container, whereas a PBN disk was used at the top. The disk used as a partition also served as a piston that transmitted pressure to the lower compartment. Here, almost pure NaCl was used to calibrate pressure.[16] This design has been used from 2008 onward, irrespective of the size of the pressure transmitting medium (i.e., irrespective of the pressure region investigated, partly because of the high price of high-precision processing of diamond materials).

It is interesting to note that the sample holder as a whole can be regarded as forming a Gibbs ensemble.[17] The surroundings constitute a heat as well as a pressure reservoir, and the latter is kept at p_{ex}. The PBN cover at the top of the holder starts to transmit pressure when the temperature rises beyond ~500 K. At around this temperature, the pressures between the upper and lower compartments separated by the movable piston equilibrate. This was confirmed by a blank experiment in which both compartments were filled with a pressure calibrant. Thus, p_{ex} is an upper bound that p_{in} approaches from below upon heating. That is, pressure loading toward p_{ex}, which is

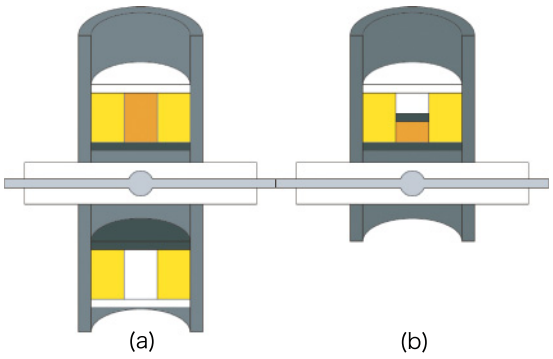

FIG. 3. (Color online) Sectional views of the graphite tube used as a heater and the corundum tube (enveloping the thermocouple) inserted through it. This is stored in the central part of the pressure-transmitting medium shown in Fig. 1. The sample container consists of a diamond sleeve and covers, one of which is a diamond disk and the other is a PBN disk. (a) Two containers are placed symmetrically around the corundum tube. One is filled with SnI_4 and the other with the pressure calibrant. The typical length of the graphite tube is 6.4 mm, and it is designed to fit into a pressure-transmitting medium with a side length of 13 mm. (b) A graphite tube of 3.6 mm length, designed for smaller pressure-transmitting media; it cannot contain two containers, and hence a single container is placed and the hollow is partitioned into the two parts by a movable thin diamond disk (which also acts as a piston). This design requires a diamond sleeve and an internal disk processed with high precision. In both cases, the remaining space in the graphite tube is filled with *h*-BN spacers. A small pellet of a pressure calibrant is usually placed immediately below the (upper) container.

"preset" at RT by actual loading, is achieved just by heating. Figure 4 shows examples of the variation of the pressures.

Before moving to the next section, we should stress that the design of the sample holding was intended to stably hold a liquid sample. It can indeed keep a liquid SnI_4 for more than a day. If the sample to be held is in solid state, the situation becomes simpler. The cover at the bottom of the holder may be replaced by a PBN disk, whereupon more effective transmission of pressure can be expected.

III. RESULTS

In this section, structural data of CP-I obtained from the sample held in the aforementioned manner along thermodynamic paths were provided for the analysis to establish the EOS. The 12 sets of data mentioned at the beginning of the previous section fall into three categories. The first category consists of data taken before 2005 using an ordinary sample container.[10] The second and third categories consist of the data obtained by using the types of sample holdings shown in Figs. 3(a) and 3(b), respectively. As noted in the previous section, the data in the third category that were taken below 500 K were not used in the analysis as the internal pressures measured within the container with the pressure calibrant are no longer reliable because of the insufficient ability of the PBN cover to transmit pressure at low temperatures. Variations in the specific volume of CP-I against changes in p and T were locally smoothed or interpolated in a suitable manner, if necessary, before processing.

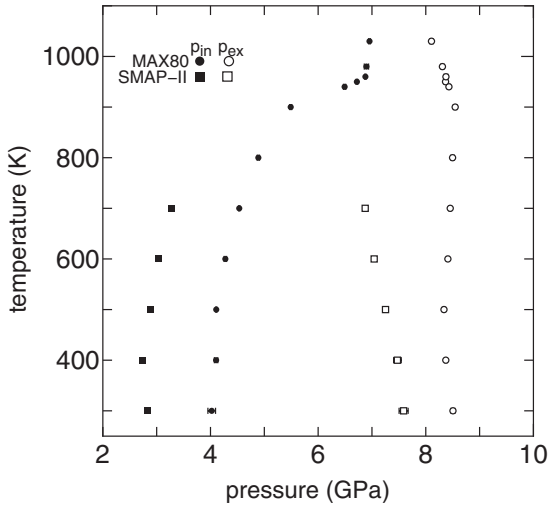

FIG. 4. Two examples showing a quite interesting feature of PBN regarding its ability to transmit pressure. One (marked by circles) is from an experiment using MAX-80, and the other (marked by squares) is from an experiment using SMAP-II. The ability, and therefore the internal pressure, p_{in}, increases with temperature. In particular, it is remarkably enhanced after melting the sample at 900 K until it is saturated at around 1000 K. The external pressure, p_{ex}, was monitored by a pressure calibrant that was placed immediately below the sample container.

We first outline our procedure for analysis, and begin with analyzing the compression behavior at RT. Three equations of state were applied, namely Murnaghan's EOS,[18] the Birch-Murnaghan (BM) EOS,[2] and the Parsafar-Mason (PM) EOS.[19] Here, because the same data set was provided for the analysis, the differences in the resultant bulk moduli and their pressure derivatives may be ascribed to the different equations adopted. The results also allow a comparison with results obtained by other researchers who used the same EOS but different pressure zones. After establishing the EOS at RT, the EOS at elevated temperatures was constructed. Care had to be taken in the construction, because the specific volumes available were not uniformly distributed on the p-T plane within the CP-I phase field. Here, we invoked the same procedure as that employed in the construction of the EOS of h-BN from its limited structural data.[20] To this end, we first fitted our structural data at elevated temperatures to the PM EOS.[19] We then extracted from the result an estimate for $\partial p/\partial T$, which is used to evaluate thermal pressure according to the treatment shown by Anderson *et al.*[21] The thermal pressure term thus estimated is simply added to the BM EOS[2] to yield the EOS available at elevated temperatures. We call the latter EOS the Birch-Murnaghan-Anderson (BMA) EOS in this paper. The quality of this EOS, together with the PM EOS, is examined in the next section by comparing their predictions with the recent experimental results.

A. EOS at RT

The Murnaghan[18] and the BM[2] equations of state are both well known. Although the name Murnaghan is common to both equations, the physics behind them is completely different; the latter EOS was derived from the thermodynamic relation using the elastic strain energy expressed in terms of *finite strains*, whereas the former is said to be an *infinitesimal strain* EOS. Hence, the Murnaghan EOS involves less physical content, but is still attractive because of its mathematical clarity.

The PM EOS[19] has, on the other hand, a quite different basis; it is based on the ingenious observation of Parsafar and Mason that the binding energy in the repulsive region (which dominates the compression behavior of a material) can generally be represented by a cubic expansion in the density. This consideration was ingeniously extended to express the thermodynamic potential, from which the EOS was derived. The PM EOS is known to have wide applicability to various materials, not only in the solid but also in the liquid state.[22]

For completeness, the forms of the equations relevant to the following discussion are given below. A general solution to Murnaghan's EOS was derived in Ref. 23; the first- and second-order equations of state are

$$p = \frac{K_0}{K_0'}(v^{-K_0'} - 1), \tag{2}$$

and

$$p = -\frac{\sqrt{|D|}}{K_0''}\frac{\left[1 + \left(\frac{K_0'}{\sqrt{|D|}}\right)^2\right]\tan\left(\frac{\sqrt{|D|}}{2}\ln v\right)}{1 + \frac{K_0'}{\sqrt{|D|}}\tan\left(\frac{\sqrt{|D|}}{2}\ln v\right)}, \tag{3}$$

with $D = {K_0'}^2 - 2K_0''K_0$, respectively. Here, $v \equiv V/V_0$ is the specific volume defined by the ratio of the volume V to that at ambient conditions. The subscript 0 in the bulk modulus and its pressure derivatives denote that they are evaluated at ambient pressure. The BM EOS takes the form

$$\begin{aligned} p &\equiv P_{\mathrm{BM}}(v, T = 300\ \mathrm{K}) \\ &= \tfrac{3}{2}K_0(v^{-7/3} - v^{-5/3})[1 - \zeta(v^{-2/3} - 1)], \end{aligned} \tag{4}$$

where $\zeta = \frac{3}{4}(4 - (\partial K_T/\partial p)_T)$ was, in addition to K_0, treated as a fitting parameter. Finally, the PM EOS is given by the form

$$p_{\mathrm{PM}} = A_0 v^{-2} + A_1 v^{-3} + A_2 v^{-4}, \tag{5}$$

where the coefficients A_0, A_1, and A_2 are functions of T. Here, we always measure the pressure in units of GPa. We require that Eq. (5) should satisfy the relation

$$A_0 + A_1 + A_2 = 0 \tag{6}$$

at ambient conditions. Henceforth, Eq. (5), on which Eq. (6) is imposed, is referred to as the constrained PM (CPM) EOS, whereas Eq. (5) without the constraint is referred to as the unconstrained PM (UPM) EOS.

Fitting was done by nonlinear regression analysis. The quasi-Newton (QN)[24] and the Rosenbrock pattern search (RPS)[25] methods were employed for the regression. In the analyses performed, the QN always took us to a global minimum that was independent of the initial guess for the parameters in the parameter space, whereas a solution from the RPS was often trapped in a local minimum near the initial guess. The latter feature is not necessarily a disadvantage in determining the parameters at elevated temperatures, as noted in the next subsection.

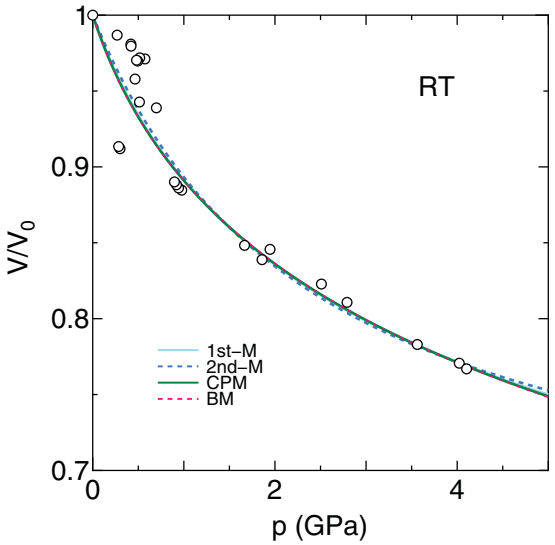

FIG. 5. (Color online) Compression data (marked by open circles) of the CP-I structure of SnI_4 at RT. The data are fitted to the various equations of state, as indicated [1st M: first-order Murnaghan, Eq. (2), 2nd M: second-order Murnaghan, Eq. (3), CPM: constrained Parsafar–Mason, Eq. (5) with (6), and BM: Birch–Murnaghan, Eq. (4)]. Note that all the curves are almost indistinguishable from one another.

Figure 5 shows the compression curves at RT as determined by fitting the compression data (shown by circles) to the Eq. (2) through (5) with (6). The data obtained below 1 GPa are relatively scattered because the sample holder was made of hard materials that prevented applied pressure from being evenly distributed inside unless it was above a threshold. That is, at low pressure, the actual pressure that was transmitted into the container was dependent on the condition of the container.[26] Although the plots almost converge into a single curve at first glance, the resultant sets of values for the bulk moduli and their pressure derivatives (see Table I) are roughly classified into two groups, one resulting from fitting to a two-parameter EOS and the other from fitting to a three-parameter EOS. At any rate, a small value such as $K_0 \simeq 5$ GPa reflects extreme softness of CP-I. This feature, along with comparison with other measurements, will be discussed in the next section.

B. EOS at elevated temperatures

First, the compression data were rearranged along the isotherms for every 100 K from 300 K (RT). Then, as outlined at the beginning of this section, the data (except that at 400 K) were fitted to the UPM EOS, Eq. (5). The QN method tends to search for a global minimum in the parameter space. That is, it tries to find on the whole surface of $p_{\rm PM}$ a part that can best fit to an isotherm under consideration. Therefore, we looked for a part of the UPM surface whose isotherm at RT coincided with the one described by the CPM EOS at RT already obtained above. It was useful to employ the RPS method to this end, making use of the fitting result for $\{A_i\}$ at the lower temperature as initial input.

Figure 6 shows the selected isotherms fitted to the data points in this manner. The difference in the pressure at different temperatures is very subtle, especially at around $v \sim 0.75$, near RT. This makes the fitted isotherms almost contact each other at around this point. Fortunately, however, meaningful information regarding $\partial p/\partial T$ is anticipated to be extracted at around $v = 1$. Indeed, the pressures at $v = 1$ are plotted against T in the inset. From this plot, an almost linear dependence of the pressure on T emerges. Thus, the points are fitted to a line (shown), whose slope yields $(\partial p/\partial T)_{v=1} = 6.75 \times 10^{-4}$ GPa/K. This will be used as input to evaluate a contribution to the thermal pressure, which is added to the BM EOS at RT.

The bulk modulus and its pressure derivative at ambient pressure are readily obtained from Eq. (5), and are related to the coefficients $\{A_i(T)\}$ in the following way:

$$K_{0T} = 2A_0 + 3A_1 + 4A_2$$
$$K_{0T}{}' = -1 + (6A_0 + 12A_1 + 20A_2)/K_{0T}. \qquad (7)$$

The values for K_{0T} obtained through Eq. (7) are summarized in Table II. Reliable error estimation could not be performed in this case. However, a very slight "hardening" with increasing temperature is noticeable. The derivatives also change slightly: ${K_0}'_T \simeq 8$ ($T \leqslant 700$ K) and ${K_0}'_T \simeq 7$ ($T \geqslant 800$ K).

We are now at the stage of completing the EOS by supplementing to Eq. (4) the thermal pressure contribution assessed by the information hitherto obtained. To do this, we follow the treatment by Anderson *et al.*,[21] who regarded $(\partial K_T/\partial T)_V$ as a constant. The thermal pressure, which should be added to Eq. (4), is then derivable from two thermodynamic identities: $(\partial p/\partial T)_V = \alpha K_T$ and

TABLE I. The bulk moduli and their pressure derivatives at ambient conditions obtained through the fitting of the compression data shown in Fig. 5 to the equations of state. The large scatter of the data prevented us from making a reliable error estimate except for the fitting to the BM EOS. The QN and RPS methods gave the same results except for the fit to the second-order Murnaghan EOS, in which three parameters were involved. The values in the table were from the QN method. The RPS method yielded the same K_0, but ${K_0}' = 2$, ${K_0}'' = 3$ GPa^{-1}. The number in brackets indicates the accuracy of the last digit.

EOS	K_0 (GPa)	${K_0}'$	${K_0}''$ (GPa^{-1})
1st M	6	7	—
2nd M	7	4	1
BM	5.2(9)	9(2)	—
CPM	5	8	—

TABLE II. The bulk moduli at elevated temperatures evaluated at ambient pressure from two equations of state: UPM EOS [Eq. (5)] and BMA EOS [Eq. (8)]. Although associated errors could not be estimated for the former, the results seem to coincide with each other. A very slight increase in K_{0T} with heating is noticeable.

	K_{0T} (GPa)	
T (K)	UPM	BMA
500–700	5	5(1)
800-900	6	6(1)

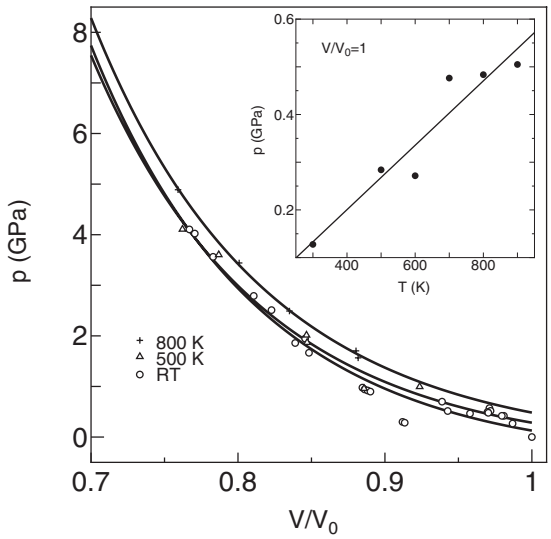

FIG. 6. Fit of the compression data at elevated temperatures to the UPM EOS, Eq. (5). To avoid unnecessary complexity, three sets of data along an isotherm at the temperature indicated are shown with the fitted curves. (The curves are extended to a high-pressure region beyond the CP-I phase field.) Inset: The pressures at $v = 1$ are almost linearly dependent on T as fitted to the line whose slope yields $(\partial p/\partial T)_{v=1} = \alpha K_T(v = 1,T) = 6.75 \times 10^{-4}$ GPa/K. The latter equality is provided for an estimate of the thermal pressure contribution in the following.

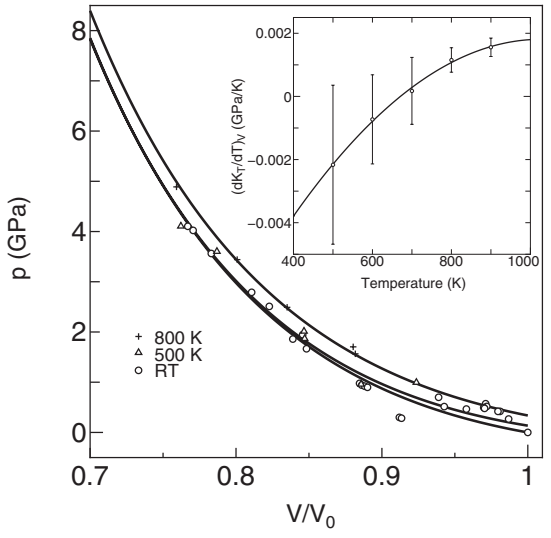

FIG. 7. The same compression data as shown in Fig. 6 are fitted to the BMA EOS, Eq. (8), regarding $(\partial K_T/\partial T)_V$ as a fitting parameter. The values for the parameter are plotted against temperature in the inset. The curve in the inset is a quadratic function of temperature, which can capture the variation in $(\partial K_T/\partial T)_V$.

$[\partial(\alpha K_T)/\partial V]_T = -(1/V)(\partial K_T/\partial T)_V$, where $\alpha = (1/V)(\partial V/\partial T)_p$ is the coefficient of thermal expansion. Equation (4) is thus extended as

$$p_{\rm BMA}(v,T) - p(v = 1, T = 300\ {\rm K}) = p_{\rm BM}(v, T = 300{\rm K}) + \left[\alpha K_T(v = 1,T) - \left(\frac{\partial K_T}{\partial T}\right)_V \ln v\right](T - 300), \quad (8)$$

where $p(v = 1, T = 300\ {\rm K})$ is negligible (when measured in units of GPa), and $(\partial K_T/\partial T)_V$ is treated as a fitting parameter. As for $\alpha K_T(v = 1,T)$, $(\partial p/\partial T)_{v=1} = 6.75 \times 10^{-4}$ GPa/K is substituted regardless of temperature (see Fig. 6).

Then, since only one parameter in Eq. (8) was at our disposal, a meaningful error estimate was made, and both QN and RPS methods gave the same results within the error. The aspect of the fit for the selected isotherms is depicted in Fig. 7. Although the isotherms at RT and 500 K seem to merge in the high-pressure region, the behavior is not unusual compared with that seen in Fig. 6.

The resultant values for the parameter are plotted against T in the inset. $(\partial K_T/\partial T)_V$ varies from negative to slightly positive (i.e., normal to less normal) values with temperature, although the absolute values are extremely small.[27] However, their variation is relatively smoother, and is well described by a quadratic curve

$$(\partial K_T/\partial T)_V = -1.32 \times 10^{-2} + 2.92 \times 10^{-5} T - 1.42 \times 10^{-8} T^2, \quad (9)$$

as delineated in the inset. Note that we consider $(\partial K_T/\partial T)_V$ to be virtually volume independent.

Equations (8) and (9) complete the construction of the BMA EOS expected to be valid at arbitrary (v,T) points in the CP-I phase field. The validity of the BMA EOS is examined in the next section.

IV. DISCUSSION

At RT, $K_0 \simeq 5$ GPa and $K_0{}' \simeq 8$ were obtained in our analysis. The value for K_0 was virtually indistinguishable from $K_0 = 4.98$ GPa, the value reported by Peercy *et al.*[28] Since the latter was determined from a pressure range of $0 \leqslant p \leqslant 0.3$ GPa, the initial softness of CP-I upon compression dominates in determining these results. In contrast, Grocholski *et al.* reported $K_0 = 10.6(1)$ GPa and $K_0{}' = 4.1(1)$,[1,29] the value for K_0 being almost doubled, whereas that for $K_0{}'$ halved. A much extended pressure range of $0 \leqslant p \lesssim 15$ GPa was used in their analysis, in which a third-order isothermal Eulerian finite-strain EOS[30] was applied. Note that their values are rather close to the values we obtained by fitting to the second-order Murnaghan EOS (see Table I). Since the EOS employed by their analysis is simply the BM EOS, Eq. (4), the difference in the values for K_0 and $K_0{}'$ could be attributed to the difference in the pressure range used in the fit. Their range extends beyond the CP-I phase field, passing through the CP-II phase field to the region where amorphization starts, and therefore the values are not necessarily characteristic of CP-I.

Sato and Hamaya obtained $K_0 = 6.1(2)$ GPa and $K_0{}' = 7.6(3)$ from precise measurements of the volume within the CP-I phase field up to 6.6 GPa.[31] They used Vinet's EOS,[32] with V_0 being fixed at 1847 Å^3/unit cell. Hence, K_0 and $K_0{}'$ were the only parameters at their disposal. These values for K_0 and $K_0{}'$ are reliable, because their measurements were done entirely under hydrostatic conditions using a fluid as a pressure-transmitting medium. Our measurements, as well as those of Peercy *et al.*, resulted in a somewhat lower value of K_0,

TABLE III. Comparison of the pressures calculated from the various equations of state mentioned in the text with those obtained through measurement at RT (listed in the "Exp" column). The experimental data belong to the oldest category mentioned in Sec. III. The same abbreviations introduced in Fig. 5 were used for the equations of state; SH and GSJ denote the equations of state reported in Refs. 1 and 31, respectively.

	Pressure at RT (GPa)						
v	Exp	1st M	2nd M	BM	CPM	SH	GSJ
0.909(1)	0.96(2)	0.8	0.8	0.8(2)	0.8	0.83(4)	1.22(2)
0.876(1)	1.00(1)	1.2	1.2	1.2(3)	1.2	1.33(7)	1.84(3)
0.821(1)	2.16(3)	2.3	2.3	2.4(7)	2.4	2.48(15)	3.12(6)
0.769(1)	3.90(9)	4.1	4.1	4(1)	4.1	4.18(29)	4.78(11)

because shear components were involved in the deformation induced under nonhydrostatic conditions.

Before discussing the thermodynamic behavior at elevated temperatures on the basis of Eqs. (8) and (9), the justification for choosing BM EOS, Eq. (4), as the reference EOS at RT should be examined. A comparison of the differences between the pressures calculated from the equations of state mentioned in the preceding paragraphs and those studied in Sec. III A is useful in the examination. The empirical relationship of Peercy *et al.*[28] describing the compression behavior in the infinitesimal strain limit is not applicable in the cases for $v \leqslant 0.97$ (i.e., to the principal part of our data shown in Fig. 5) as far as their fitted parameters are used. The value of $K_0 = 4.98$ GPa mentioned earlier was obtained from the latter parameters.

The pressure values obtained from the other equations of state for the values of v indicated in Table III are listed in the same table. The measured values for p are also included. The experimental data for v and p were taken from a set that belongs to the oldest category, the classification described in Sec. III. As can be seen from Table III, the EOS given by Grocholski *et al.*[1] yields systematically higher pressure values, whereas pressure values obtained from the other equations of state are virtually indistinguishable from one another. The large scattering of the compression data in the low-pressure region in Fig. 5 had almost no effect on determining the parameters involved in the latter equations of state, i.e., the functional behavior of the latter equations of state was primarily determined in a region of relatively large deformation. If we regard the scattering Δv in the specific volume in Fig. 5 as a reflection of the inhomogeneity of the actual strain field, the EOS in the latter group yields the ambiguity, Δp in p due to Δv, which decreases with increasing p in such a way that $|\Delta p| \simeq 0.7$ GPa when $p \simeq 0.3$ GPa, whereas $|\Delta p| \simeq 0.07$ GPa when $p \simeq 2$ GPa. Thus, the EOS of Grocholski *et al.* shows a marginal behavior. This is because their EOS focuses on a much higher pressure zone, where solid-state amorphization starts to occur. Hence, as far as the EOS at RT for CP-I is concerned, the reference should be chosen from the latter group.

Although Murnaghan's (infinitesimal-strain) equations of state, Eqs. (2) and (3), yield a similar compression behavior, these were excluded from the reference EOS because they were no longer based on the infinitesimal deformation data. (However, it is highly expected that the compression data of Peercy *et al.*,[28] if available, would lie closely on the curves of Murnaghan's EOS with the parameters listed in Table I.) The CPM EOS, Eq. (5) with Eq. (6), was also excluded because it was already used at the initial stage of extracting the value for $(\partial p/\partial T)_{v=1}$.

The Sato-Hamaya (SH) EOS,[31] based on the finite-strain EOS of Vinet *et al.*,[32] was thus one of the candidates for a reference EOS other than the BM EOS. Although the SH EOS was derived from measurements performed under hydrostatic conditions, we chose the BM EOS, Eq. (4), as the reference here [see Eq. (8)] because, as far as the nonhydrostaticity is concerned, all our data were obtained under the *same* environment. That is, by choosing BM EOS as the reference, we intended to be consistent over the whole analysis. It is easily inferred from the pressure differences listed in Table III that the final EOS would be virtually the same if the reference adopted had been SH EOS.

At elevated temperatures, CP-I shows a somewhat odd compressibility behavior. As far as can be seen from the value for K_{0T} (see Table II), it becomes slightly hardened. This unusual behavior was extracted from a trial fit of the specific volumes at elevated temperatures to the UPM EOS. Considering that this slight increase in K_{0T} occurs near the melting point of CP-I, the compression behavior near a phase transition point seems beyond the capability of the PM EOS description (although the EOS can capture the compression behavior within a single condensed phase), and hence the "hardening" is apparent.[33] This feature is propagated through the nonzero $(\partial p/\partial T)_V = \alpha K_T$ to the behavior of the thermal pressure in the BMA EOS.

The slight change in K_T with temperature implies that thermal pressure is volume dependent, as evident from the thermodynamic identity used in the last section. The temperature dependence of K_T derived from Eq. (8) enters only through the thermal pressure term. Then, $\partial K_T/\partial T = \partial/\partial T[(\partial K_T/\partial T)_V(T - 300)]$ depends only on T if $(\partial K_T/\partial T)_V$ in the thermal pressure is virtually volume independent, as we assumed. This means that $(\partial K_T/\partial T)_V$ is virtually the same as $(\partial K_T/\partial T)_p$. This is not inconsistent with our situation as shown from a thermodynamic relationship $(\partial K_T/\partial T)_V - (\partial K_T/\partial T)_p = (\partial K_T/\partial p)_T \alpha K_T$ whose right-hand side takes a small value such as $\sim 5 \times 10^{-3}$ GPa/K irrespective of T. However, this causes a severe inconsistency in the above equation regarding $\partial K_T/\partial T$ unless $(\partial K_T/\partial T)_V$ is a temperature-independent constant. In this context, Eq. (8), when supplemented by Eq. (9), is no more than phenomenological.

The three sets of internal pressures measured in recent experiments, in which the type of sample holder shown in Fig. 3(b) was employed, are listed in Table IV. (For the data sources, refer to the caption.) The predictions given from Eq. (8) with Eq. (9) when measured T and v were used as input are also included. The maximum deviation was found for the small compression at RT. However, this is partly ascribed to the nonuniqueness of the measured internal pressure at RT when the applied pressure was not large enough, as mentioned in Sec. III. In fact, this was not the case for another measurement at RT and $v \sim 1$. Except for this, the deviation is said to be within roughly 0.1 GPa. The agreement between

TABLE IV. Comparison of the pressure predicted by the equations of state and the one directly measured. Three sets of experimental runs are given, and are denoted by B194, B213, and A1285. The first two runs are the *in situ* measurements performed in 2009 and 2011 using SMAP-I (which has a similar architecture to SMAP-II mentioned in Sec. II) installed in BL22XU at SPring-8, Japan. The third run is the measurement performed in 2009 using SMAP-II. T and v are the temperature and the specific volume, respectively, on a thermodynamic path along which the pressure, $p_{\rm in}$, was measured using the single-container type of sample holding illustrated in Fig. 3(b). These pressures are listed in the column denoted "Exp". The values for T and v were used as input to the BMA and UPM equations of state, given by Eq. (8) with Eq. (9) and Eq. (5), respectively. The pressures output from these equations of state are listed in the corresponding columns.

	Condition		Pressure (GPa)		
	T (K)	v	Exp	BMA	UPM
B194	300	0.9860(5)	0.099(11)	0.08	0.20
	300	0.9640(14)	0.285(10)	0.23	0.34
	400	0.9673(19)	0.321(18)	0.26	0.40
	450	0.9667(3)	0.350(16)	0.29	0.45
	500	0.9686(3)	0.407(15)	0.31	0.47
	550	0.9723(3)	0.415(10)	0.33	0.49
	600	0.9777(3)	0.423(27)	0.33	0.49
B213	300	0.9347(32)	0.727(10)	0.48	0.58
	400	0.9250(21)	0.662(9)	0.61	0.75
	500	0.9205(5)	0.815(9)	0.72	0.88
	600	0.9179(7)	0.947(24)	0.84	0.99
	700	0.9170(4)	1.053(18)	0.94	1.09
	800	0.9158(6)	1.221(13)	1.06	1.19
	850	0.9137(8)	1.273(22)	1.14	1.27
A1285	300	0.8573(22)	1.56(1)	1.56	1.59
	300	0.8390(25)	1.99(2)	1.94	1.95
	300	0.7981(19)	2.83(3)	3.04	2.99
	600	0.8022(6)	3.04(3)	3.06	3.07
	700	0.7972(22)	3.27(4)	3.36	3.35

the predictions and the measurements improves significantly as compression proceeds. This comparison shows that Eq. (8) with Eq. (9) can be adopted for practical use. This also means that the EOS properly captures—though quite roughly—the essential thermodynamic behavior of CP-I.

Finally, we reexamine the PM EOS, and quantitatively evaluate its thermal pressure contribution at elevated temperatures. The temperature dependences of the coefficients $\{A_i\}$ of the UPM EOS obtained through the fit illustrated in the isotherms in Fig. 6 were extracted by trying to fit $\{A_i\}$ to the quadratic functions

$$A_i(T) = \sum_{j=0}^{2} a_{ij} T^j. \tag{10}$$

The result was: $a_{00} = 4.09$ GPa, $a_{01} = -1.51 \times 10^{-3}$ GPa K^{-1}, $a_{02} = 2.07 \times 10^{-6}$ GPa K^{-2}; $a_{10} = -1.43 \times 10$ GPa, $a_{11} = 9.06 \times 10^{-3}$ GPa K^{-1}, $a_{12} = -8.04 \times 10^{-6}$ GPa K^{-2}; $a_{20} = 1.00 \times 10$ GPa, $a_{21} = -6.58 \times 10^{-3}$ GPa K^{-1}, $a_{22} = 5.72 \times 10^{-6}$ GPa K^{-2}. The resultant surface of $p_{\rm PM}$, given by Eq. (5) with Eq. (10), was almost indistinguishable from that of $p_{\rm BMA}$. The values of $p_{\rm PM}$ corresponding to the sets of (v,T) used in the inspection of $p_{\rm BMA}$ are also given in Table IV. The agreement between $p_{\rm PM}$ and $p_{\rm in}$, directly measured, was similar to (or sometimes better than) that between $p_{\rm BMA}$ and $p_{\rm in}$. This quality of agreement was caused by a fortunate series of error cancelations during the processing. Since the temperature dependence of $\{A_i\}$ was originally introduced on a phenomenological basis,[19] no attempt was made to extract further information from Eq. (10) here.

In view of the EOS, CP-I behaves as a normal solid (except in the vicinity of the melting point). The thermodynamic properties of CP-I are, in principle, understood on the basis of weak (physical) interactions between the molecules.[34] The intriguing feature of the polyamorphic transitions is triggered by some chemical interaction between intermolecular iodine atoms. The latter interaction will be activated when the intermolecular iodine atoms are brought closer to each other, beyond the distance between intramolecular iodine atoms.[13] This close approach is realized by an external pressure. A lower pressure is required in the liquid state, because not only displacements but also rotations are available for the molecules to shorten the relevant distance. Such a microscopic situation will also give rise to an anomaly in macroscopic properties. In this context, the EOS of the liquid state[35] should also be reexamined, in particular under high-density conditions.

V. CONCLUSION

The EOS of CP-I was examined and was found to be practically described by the BMA form of Eq. (8) supplemented by Eq. (9). An EOS of similar quality was obtained from the PM form, Eq. (5). The validity of these equations was confirmed by several measurements. Although these equations of state were constructed on a phenomenological basis, we believe that they are practically useful over the entire CP-I phase field.

From the equations of state, $K_0 \simeq 5$ GPa and $K_0{}' \simeq 8$ were obtained for CP-I at RT. These values were close to those obtained under hydrostatic conditions.[31] Little change has been observed in the bulk modulus and its pressure derivative with heating up to near the melting point, where a slight "hardening" was noticeable. No other anomaly was found in view of the behavior of the equations of state. The volume data of CP-I obtained through *in situ* x-ray diffraction measurements enabled us to construct the equations of state. These measurements were realized by a unique manner of sample holding illustrated in Sec. II.

ACKNOWLEDGMENTS

Many researchers and graduate students were involved in the projects performed at SPring-8 and KEK-AR, Japan. Among them, special thanks are due to Y. Katayama, T. Kikegawa, A. Yamada, T. Hase, T. Sakagami, Y. Yamagata, and F. Matsuura for their assistance. The data used in this research are from the work performed at SPring-8 under Proposal Nos. 2001B0160-ND-np, 2002A0103-CD2-np, 2009A3614, 2009B3782, and 2010B3781, and at KEK-AR under 2006G035, 2008G078, and 2010G032. K.F. was supported by a Grant-in-Aid for Scientific Research from the Ministry of Education, Culture, Sports, Science and Technology of Japan (Grant Nos. 22540392 and 23103703).

*fuchizak@phys.sci.ehime-u.ac.jp

[1]B. Grocholski, S. Speziale, and R. Jeanloz, Phys. Rev. B **81**, 094101 (2010).

[2]F. Birch, J. Geophys. Res. **57**, 227 (1952).

[3]N. Hamaya, K. Sato, K. Usui-Watanabe, K. Fuchizaki, Y. Fujii, and Y. Ohishi, Phys. Rev. Lett. **79**, 4597 (1997). One of the important achievements in this work was the discovery of two amorphous states with different densities, which are solid-state counterparts of the two liquids found in Ref. 13. As for the structural analysis of the high-density amorphous state, see Ref. 6.

[4]M. Riggleman and H. G. Drickamer, J. Chem. Phys. **38**, 2721 (1963).

[5]Y. Fujii, M. Kowaka, and A. Onodera, J. Phys. C **18**, 789 (1985).

[6]A. Ohmura, K. Sato, N. Hamaya, M. Isshiki, and Y. Ohishi, Phys. Rev. B **80**, 054201 (2009).

[7]K. Sato, Ph.D. Thesis, Ochanomizu University, 2000. The first-principles calculation (S. Ohta and S. Tsuneyuki, in *Proc. 3rd Symposium on Atomic-scale Surface and Interface Dynamics* (Japan Society for the Promotion of Science, Tokyo, 1999), p. 303) suggested that the structure was formed by a substitutional solid solution of Sn into fcc I sites. Such a structural feature appearing under extremely high pressures bears a striking resemblance to that of I_2, as do the electronic properties. In fact, the superconducting transition was observed at 64 GPa and 1.96 K by N. Takeshita *et al*., J. Phys. Soc. Jpn. **65**, 3400 (1996).

[8]P. Dawson, Spectrochim. Acta **31A**, 1101 (1975); I. U. Heilmann, D. J. Lockwood, and G. S. Pawley, J. Phys. C **11**, 1699 (1978).

[9]I. U. Heilmann and N. B. Olsen, in *Proceedings of the International Conference on Lattice Dynamics*, edited by M. Balkanski (Flammarion, Paris, 1978), p. 475.

[10]K. Fuchizaki, Y. Fujii, Y. Ohishi, A. Ohmura, N. Hamaya, Y. Katayama, and T. Okada, J. Chem. Phys. **120**, 11196 (2004).

[11]F. E. Simon, Nature (London) **172**, 746 (1953).

[12]The striking resemblance of the aspect of the melting curve to that of black phosphorus [Y. Katayama, T. Mizutani, W. Utsumi, O. Shimomura, M. Yamakata, and K. Funakoshi, Nature (London) **403**, 170 (2000)] prompted us to look into the liquid region to search for a new liquid phase. This was indeed the case. See Ref. 13.

[13]K. Fuchizaki, T. Hase, A. Yamada, N. Hamaya, Y. Katayama, and K. Funakoshi, J. Chem. Phys. **130**, 121101 (2009).

[14]H. L. Suchan and H. G. Drickamer, J. Phys. Chem. Solids **11**, 111 (1959).

[15]K. Fuchizaki, S. Kohara, Y. Ohishi, and N. Hamaya, J. Chem. Phys. **127**, 064504 (2007).

[16]Because the melting temperature of SnI_4 is much lower than that of NaCl under pressures beyond $\sim$1.5 GPa, SnI_4 must be located beneath NaCl. As is usual for a pressure calibrant, *h*-BN is mixed with NaCl to suppress its accelerated grain growth at high temperatures. However, we avoided using *h*-BN, as it diffuses into the liquid SnI_4, which invades the upper compartment through the narrow gap between the movable piston and the wall of the hollow. The contamination causes deterioration in the quality of diffraction patterns of the sample as mentioned above. Using NaCl alone sometimes makes it difficult to measure its lattice constant, in particular below 1 GPa. However, among several substances we have tried, only NaCl could be used as a pressure calibrant. For example, SnI_4 was found to be easily dissolved through some catalytic reaction into I_2 and SnI_2 by MgO, which is also frequently used for pressure calibration.

[17]M. Kardar, *Statistical Physics of Particles* (Cambridge University Press, New York, 2007), p. 115; K. Fuchizaki, J. Phys. Soc. Jpn. **80**, 024003 (2011).

[18]For example, Y. Ida and H. Mizutani, in *Chikyu Kagaku* (*Earth Science*), edited by S. Akimoto and H. Mizutani (Iwanami, Tokyo, 1978), Vol. 2, p. 34 (in Japanese).

[19]G. Parsafar and E. A. Mason, Phys. Rev. B **49**, 3049 (1994).

[20]K. Fuchizaki, T. Nakamichi, H. Saitoh, and Y. Katayama, Solid State Commun. **148**, 390 (2008).

[21]O. L. Anderson, D. G. Isaak, and S. Yamamoto, J. Appl. Phys. **65**, 1534 (1989).

[22]F. J. A. L. Cruz, J. N. Canongia Lopes, and J. C. G. Calado, Fluid Phase Equilib. **241**, 51 (2006).

[23]K. Fuchizaki, J. Phys. Soc. Jpn. **75**, 034601 (2006).

[24]P. E. Gill and W. Murray, J. Inst. Math. Appl. **9**, 91 (1972).

[25]H. H. Rosenbrock, Comput. J. **3**, 175 (1960).

[26]The scattered data in the low-pressure region came from the measurement carried out after 2005 making use of the sample holding method shown in Fig. 3(a). As far as Murnaghan's equations of state are concerned, similar values for K_0, K_0' (and K_0'') resulted from the compression data without the scattered part. This suggested that no net change in other K_0 and K_0' would occur if the part were omitted.

[27]Indeed, the absolute value is one order of magnitude smaller than that of Au. See Ref. 21.

[28]P. S. Peercy, G. S. Sarama, and B. Morosin, J. Phys. Chem. Solids **36**, 1123 (1975).

[29]Throughout this paper, the value of the error corresponds to the last significant digits in the functional value.

[30]D. Heinz and R. Jeanloz, J. Appl. Phys. **55**, 885 (1984).

[31]K. Sato and N. Hamaya, Rev. High Pressure Sci. Technol. **7**, 278 (1998).

[32]P. Vinet, J. Ferrante, J. R. Smith, and J. H. Rose, J. Phys. C **19**, L467 (1986).

[33]Unlike the case in CCl_4 and CBr_4 [see J. C. W. Folmer, R. L. Withers, T. R. Welberry, and J. D. Martin, Phys. Rev. B **77**, 144205 (2008)], no signal associated with a plastic phase transition was detected in CP-I near the melting point.

[34]K. Fuchizaki, S. Sugiyama, and Y. Fujii, J. Chem. Phys. **112**, 10379 (2000); K. Fuchizaki and T. Nagai, Solid State Commun. **132**, 305 (2004).

[35]K. Fuchizaki, S. Sugiyama, and Y. Fujii, J. Phys. Soc. Jpn. **70**, 1321 (2001).